IMPROVING 5-AXIS MILLING OPERATIONS USING PROCESS MODELS

E. Budak
Manufacturing Research Lab, Sabanci University, Istanbul, Turkey

e-mail: ebudak@sabanciuniv.edu

5-axis milling is a technology used in many industries such as aerospace, automotive and die/mold for machining of complex surfaces. Cutting forces, form errors and chatter vibrations are among the most important limitations in these operations. Process models can be used for predictions and optimization in 5-axis milling. In this paper, the process models and their applications are presented. These methods are implemented in simulation software, and applied in machining of industrial parts where productivity increase for example cases is demonstrated.

Keywords
5-axis milling, process modeling

1. Introduction

5-axis milling is mainly used in machining of complex surfaces. Technology of 5-axis milling is well established where tool and work orientation is made possible by addition of two rotational axes on machine tools with different kinematic designs. Rotational axes can be on the tool or the workpiece side, or combination of both. In addition, there are several powerful CAM software with 5-axis milling solutions. However, they consider only the geometry of the process and do not include the physics in tool path generation. Hence, the process planner has no information about cutting forces, form errors and chatter vibrations which have considerable effects on the productivity and quality of the process.

Work flow that is generally followed to produce a part with 5-axis milling is presented in Fig. 1(a). First, the CAD model of the workpiece is prepared, and then the tool path is generated by selecting a machining strategy, cutting tools and process parameters in CAM. CL file, which contains all the required tool path information, is obtained as an output of the CAM. Using a post processor program, the CL file is converted into the G code (part program) which is specific to the machine tool that will be used. Physics come into the picture when the machine tool starts cutting the work material according to the uploaded G code. During the process, torque/power limits of the spindle may be reached; high cutting forces, high form errors and chatter vibrations may arise depending on the selected process parameters. In such a case, the CAM program is modified and re-run. Since this includes iterations on software (CAM) and hardware (machine tool) sides, it causes reduced productivity and lost time. Instead, process models can be added into the workflow as presented in Fig. 1(b) eliminating iterations on the hardware side by predicting problems and taking necessary precautions on the software side. In the paper, it is shown that the proposed work flow increases the productivity process and quality of the part.

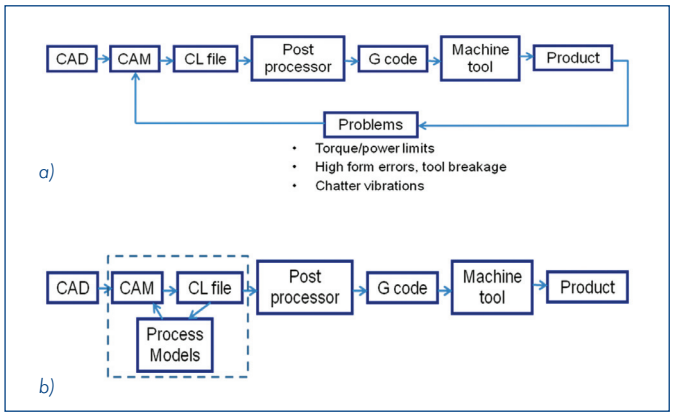

Figure 1. *(a) General work flow (b) Proposed work flow to produce a part in 5-axis milling*

There have been several works on modelling of 5-axis milling [Zhu 2001; Fussel 2003; Kaymakci 2006; Roth 2007; Budak 2009]. These works mainly differ from each other by the way cutting mechanics and engagement boundaries between tool and workpiece are modelled. Engin and Altintas [2001] modeled the cutting edge for generalized milling cutters, and used it in cutting force and stability calculations in 3-axis milling which can be extended to 5-axis milling [Ozkirimli, 2011]. However, all process models require tool-part engagement boundaries which are more complicated in 5-axis milling due to the additional degrees of freedom. The calculation of engagement limits in 5-axis milling has been mainly done using non-analytical methods. For example, Larue and Altintas [2005] used ACIS solid modeling environment to determine the engagement region for force simulations of flank milling. Kim et al. [2000] determined the engagement region using Z-mapping. Ozturk and Budak [2007], on the other hand, determined the engagement regions analytically, modeled cutting forces, tool deflections and the form errors. In another study, Lopez De Lacalle [2007] employed tool deflection calculations in selection of preferable local machining directions and tool orientation in finishing operations.

Chatter is one of the main limitations in 5-axis milling. Although chatter stability has been extensively studied, this has been very limited for 5-axis milling processes. Altintas et al. [1999] extended the analytical milling stability model [Budak, 1998] to the ball-end milling whereas Ozturk and Budak [2010] included the effect of lead and tilt angles using single and multi-frequency methods. Ozturk et al. [2009] showed the effect of lead and tilt angles on stability limits. Shamoto and Akazawa [2009] also considered the effects of tilt angle.

Various authors studied the extraction of tool-workpiece interface from a given CL file for a machining cycle. Lazoglu [2003] meshed the workpiece-cutter pair into small cubic elements and calculated the immersions at each CL point along the tool path. Ozturk and Lazoglu [2006] used CL points in order to obtain the machined surface information in 3-axis ball-end milling operations. Lopez De Lacalle, et al. [2007] integrated cutting force calculation in Unigraphics©. They directly used the CL points to approximate the curves for the tool path. In one of the recent studies Gong and Wang [2009] used moving frame method to formulate the tool swept envelope directly from CL-data which was not integrated with a force model for application on a real machining operation.

The layout of the paper is as follows. 5-axis ball-end milling geometry is presented firstly. The models used for calculation of forces and form errors are described briefly in section 3. Then, stability model used for determination of stability diagrams is presented. The stability diagram calculated by the model is compared with experiments and effects of lead and tilt angles on the absolute stability limit are shown. Finally, a method for performing full process simulations along a given tool path and its applications are demonstrated.

2. 5–Axıs mılling geometry

In order to represent position and orientation of a three coordinate systems need to be defined as shown in Fig. 2(a): The machine coordinate system (MCS) consisting of X, Y, Z axes of the machine tool; the process coordinate system (FCN) consisting of the feed

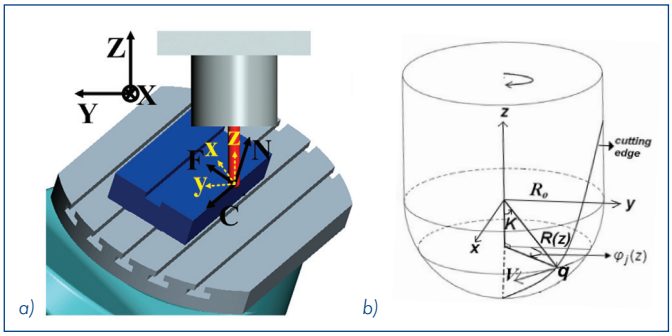

Figure 2. *(a) Coordinate systems (b) Ball-end mill geometry*

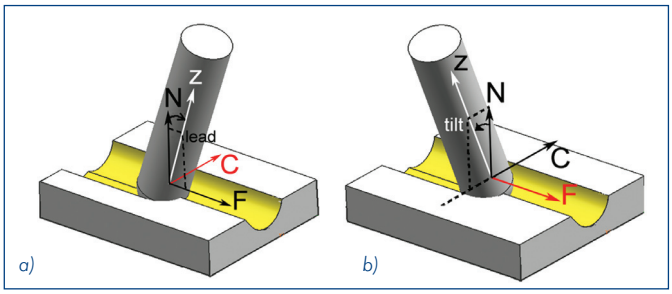

Figure 3. *(a) Lead angle (b) Tilt angle*

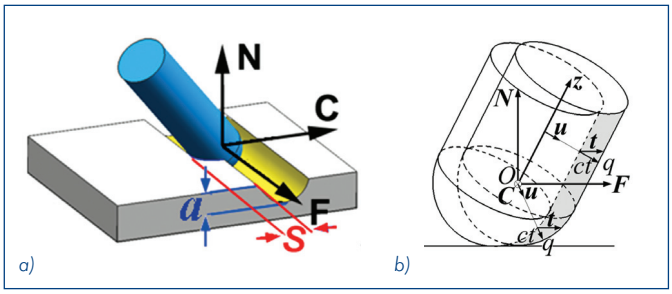

Figure 4. *(a)Cutting depth a, step over s (b)Uncut chip thickness ct*

direction (F), the cross-feed direction (C) and the surface normal direction (N); the tool coordinate system (TCS) consisting of x and y transversal axes of the tool and z along the tool axis direction. TCS defines the orientation of the cutting tool with respect to FCN. Lead angle defines the rotation of the cutting tool around C axis whereas tilt angle is the rotation of the tool around F axis (Fig. 3). Therefore, TCS is the rotated form of FCN with lead and tilt angles.

Due to the effects of lead and tilt angles, the tool axis is not parallel to the surface normal (Fig.3). Hence, the cutting depth (*a*) is the depth removed from the workpiece in the surface normal direction. The step over *s* which is the distance between the adjacent tool paths in C axis (Fig. 4(a)) defines the radial depth of cut.

Cross-feed direction is used in order to define the direction of the uncut material. If uncut material is in the positive C axis with respect to the milling tool, the cross-feed direction is positive, and vice-versa (Fig. 4(a)). Uncut chip thickness *ct* (Fig. 4(b)) is varible along the cutting edge locally in both tangential and axial directions. Local uncut chip tickness depends also on lead and tilt angles as formulated in [Ozturk, 2007] which is used on an example case where cutting depth, step over and radius of the ball-end mill are 6 mm. Helix angle on the clockwise-rotating tool is 30° and cross-feed direction is negative. The engagement for 30° lead and tilt angles are shown in Fig. 5 where the calculated engagement boundaries are also presented. Positive lead angle shifts the engagement region to higher positions along the tool axis while negative lead angle moves the engagement to lower sides of the tool. Effect of lead angle on the immersion width is presented in Fig. 6 for the same example. Norm_z is the ratio of z-coordinate with respect to ball-end mill radius. It can be seen from this figure that lower immersion widths takes place with positive lead angles.

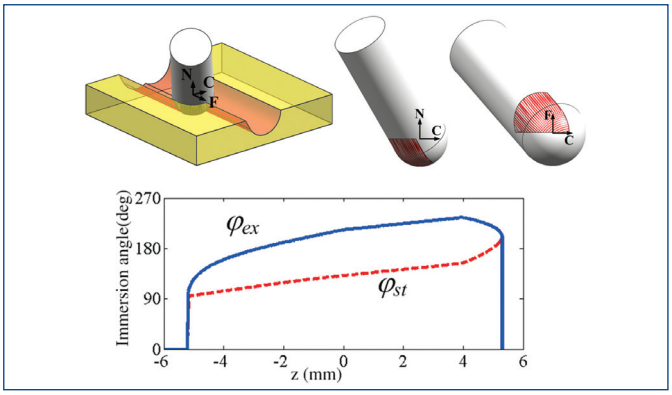

Figure 5. *Engagement region for the example case (lead,tilt=30o)*

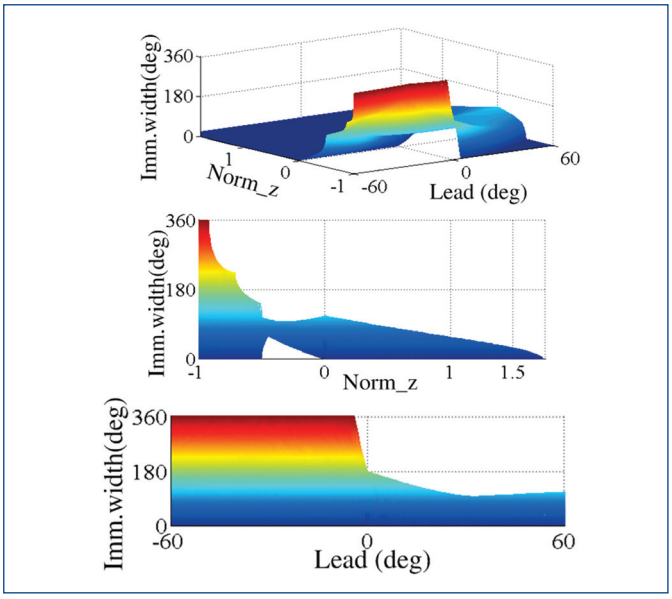

Figure 6. *Effect of lead angle on immersion width (tilt=0o)*

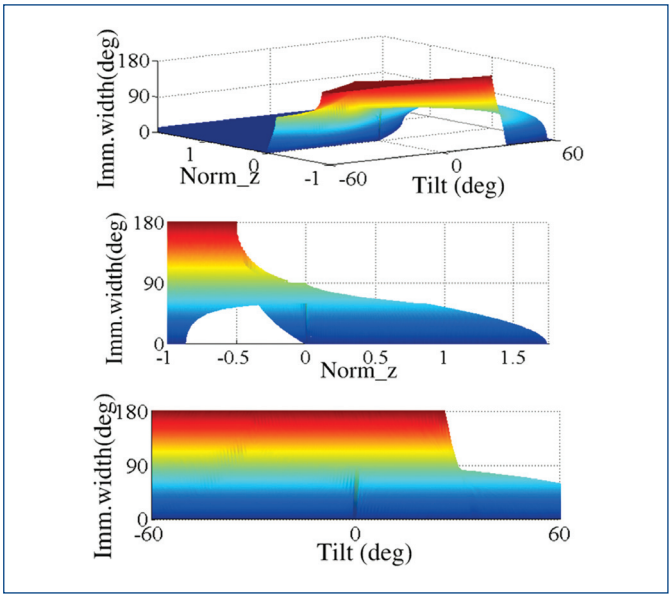

Figure 7. *Effect of tilt angle on immersion width (lead=0o)*

Effect of tilt angle is very much dependent on the cross-feed direction. If tilt angle and cross-feed direction have the same sign, the tool axis is oriented away from the uncut part of the workpiece. In this case, tilt angle decreases the z-coordinates of the engagement region. The reverse is true if the tilt angle and cross-feed direction have opposite signs. Effect of tilt angle on immersion width on different z coordinates is presented in Fig. 7 for the example case. As expected, z-coordinates of the engagement region are lower when tilt angle is negative since cross-feed direction is negative in the example case.

3. Force and Form error MODelS

After the engagement region between the cutting tool and workpiece is calculated, the oblique mechanics equations [Budak, 1996] can be applied for calculation of cutting forces. Since the geometry of the cutting tool is variable along the tool axis, cutting force coefficients are also variable locally along the cutting edge. For a representative case, variations of local chip thickness and radial cutting force coefficient along the cutting edge are presented in Fig. 8.

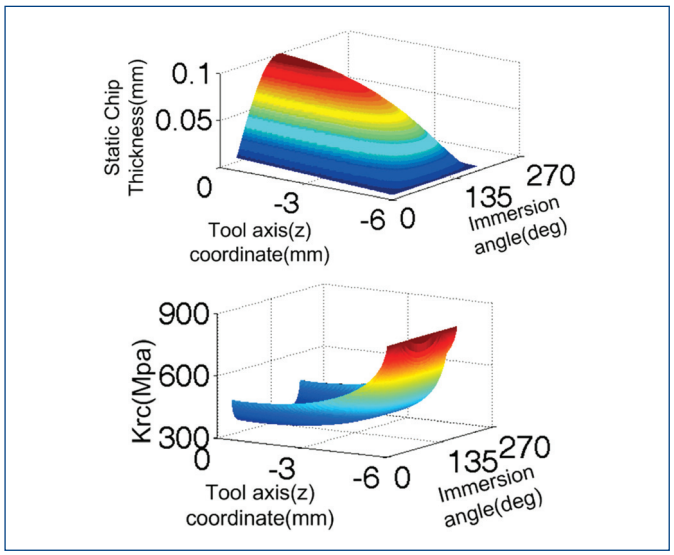

Figure 8. *Variation of (a) static chip thickness (b) radial cutting force coefficient*

In order to take the local variations into account, the cutting tool edge is divided into differential elements and on these elements following equations are written to calculate differential forces in radial, tangential and axial directions (Fig. 9a):

$$\begin{aligned} dF_{rj}(\varphi_j(z)) &= K_{re}dS + K_{rc}(ct)db \\ dF_{tj}(\varphi_j(z)) &= K_{te}dS + K_{tc}(ct)db \\ dF_{aj}(\varphi_j(z)) &= K_{ae}dS + K_{ac}(ct)db \end{aligned} \quad (1)$$

where K_{re}, K_{te}, K_{ae} are edge force coefficients and K_{rc}, K_{tc}, K_{ac} are cutting force coefficients in radial, tangential and axial directions, respectively. These coefficients are determined using corresponding orthogonal database and the oblique cutting model [Budak, 1996]. *dS* is the differential cutting edge length, *ct* is local chip thickness and *db* is the local chip width. The differential forces in *x*, *y*, and *z* directions are calculated using a geometrical transformation and finally total cutting forces in these directions are calculated by the integration of the differential forces over the engagement region [Ozturk, 2007].

For calculation of the form errors, the tool deflections at the surface generation points are determined by applying the cutting forces on the structural model of the cutting tool. The cutting tool is modelled as a beam and its connection to the tool holder, which is considered as rigid, is modelled by linear and torsional springs as shown in Fig. 9 (b) [Ozturk, 2007].

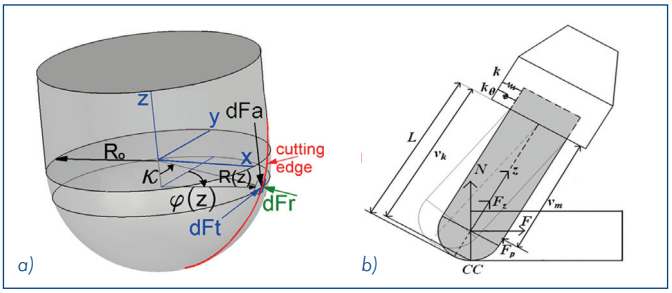

Figure 9. *(a) Representation of local cutting forces (b) Structural model of the ball-end mill*

Comparison of the results of the force model with experiments is presented in Fig. 10. The workpiece is Ti6Al4V alloy and cutting force coefficients are calculated using mechanics of milling method [Budak, 1996]. More than 70 cutting tests were performed and a statistical analysis has been performed for the prediction error of the maximum forces in *x*, *y* and *z* directions. It is seen that the error margin is less than 20% which is quite acceptable considering that no calibration has been performed for the specific tool used in the tests.

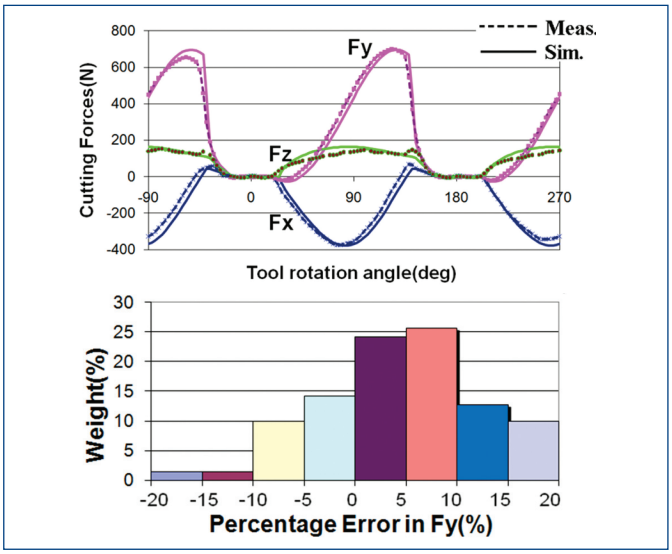

Figure 10. *Comparison of measured and simulated cutting forces*

Effect of lead and tilt angles on maximum cutting force F_{xy} is presented in Fig. 11(a) for an example case. A 12mm diameter carbide ball-end mill with 2 teeth, 8° rake angle and helix angle of 30° is used to machine Ti6Al4V alloy. The process is a following cut operation where the feed rate is 0.05 mm/tooth, the spindle speed is 1000 rpm, cross-feed direction is negative, the cutting depth and the step over are 5 mm. On the response surface three lead and tilt combinations are selected and cutting tests are performed for these cases. Measured and simulated maximum F_{xy} forces for these cases are tabulated in Table 1. It is seen that the force model predicts the effect of lead and tilt angles on maximum F_{xy} force reasonably well. In the same figure variation of simulated form error (deflection in the surface normal direction) with lead and tilt angles for another case is also presented. In this case, cutting depth and step over is 1 mm. The other process parameters are the same. For some of the lead and tilt combinations, it is worth noting that form error is negative which means that there is overcut from the surface, thus these cases should be avoided. Since cutting tools are very rigid in the tool axis direction, minimum form error is generally obtained when cutting tool axis is aligned in the surface normal direction. This is the case when lead and tilt angles are both 0° (point 1 in Fig. 11b). However, this may not

be acceptable since the tool tip is in contact with the surface leaving marks. For that reason, another lead and tilt combination according to Fig. 11 can be selected to minimize the form error.

Point	lead, tilt (deg)	Simulated max. F_{xy} (N)	Measured max. F_{xy} (N)
1	0,–40	637	600
2	30,–15	672	652
3	0,50	752	712

Tab. 1. *Simulation and measurement comparison of the cutting forces for the selected cases in Fig. 11.*

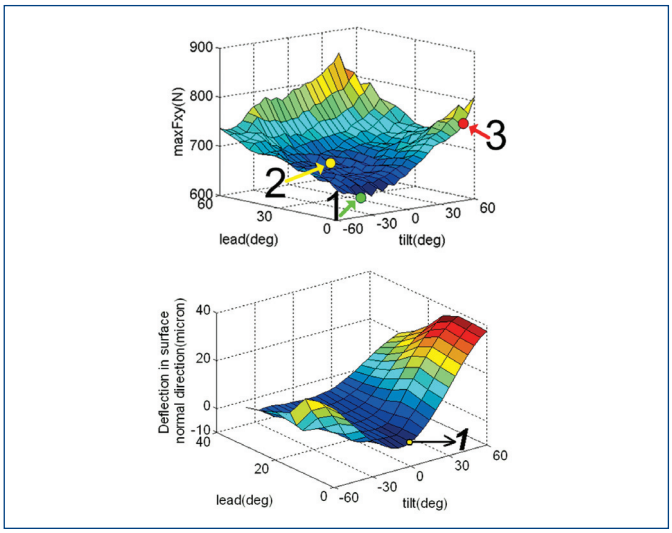

Figure 11. *Effects of lead and tilt angles on maximum Fxy force and tool deflection in the surface normal direction*

4. Chatter Stability MODel

Chatter is a regenerative vibration type which results due to the unstable interaction between dynamic chip thickness and cutting forces. In this section, formulation of 5-axis milling stability used to obtain stability diagrams is presented. The predicted stability limits are compared with experiments where the effects of lead and tilt angles on the stability are also demonstrated.

4.1 Dynamic cutting forces and stability formulation

The uncut chip thickness on the cutting edge consists of static and dynamic parts. The static part is ignored in the stability analysis since it does not contribute to the regeneration mechanism. The dynamic part h_d can be calculated by the scalar product of dynamic displacement vector d and the unit outward surface normal vector u at a cutting point on the cutting edge as follows (Fig. 12):

$$h_d = u \cdot d \tag{2}$$

The dynamic displacement vector d is the difference between the current displacements $[x_d(t),\ y_d(t),\ z_d(t)]$ and the displacements one tooth period before $[x_d(t-\tau),\ y_d(t-\tau),\ z_d(t-\tau)]$ in tool coordinate system (TCS) where τ represents the tooth period:

$$\mathbf{d} = \begin{bmatrix} \Delta x_d \\ \Delta y_d \\ \Delta z_d \end{bmatrix} = \begin{bmatrix} x_d(t) - x_d(t-\tau) \\ y_d(t) - y_d(t-\tau) \\ z_d(t) - z_d(t-\tau) \end{bmatrix} \tag{3}$$

Unit outward surface normal vector u at a point on the cutting edge can be calculated in terms of local radius $R(z)$ and local immersion angle $\varphi_j(z)$:

$$\mathbf{u} = \begin{cases} \frac{1}{R_o}\begin{bmatrix} R(z)\sin(\varphi_j(z)) & R(z)\cos(\varphi_j(z)) & z \\ \sin(\varphi_j(z)) & \cos(\varphi_j(z)) & 0 \end{bmatrix} & z \le 0 \\ & z > 0 \end{cases} \tag{4}$$

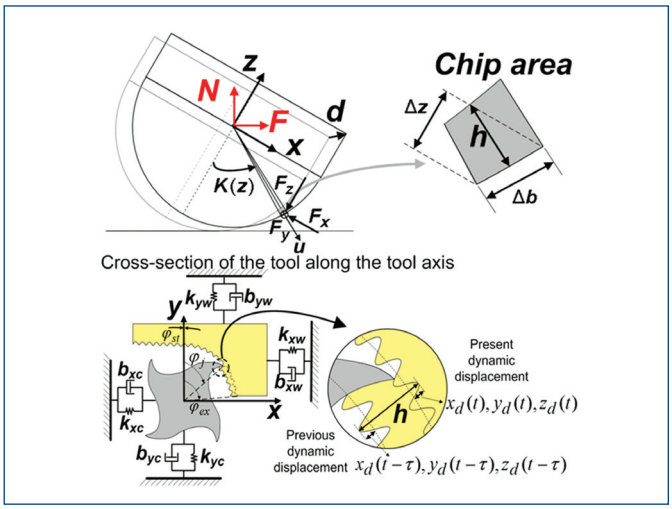

Figure 12. *The dynamic chip thickness and the regenerative effect*

As presented in section 3, the cutting force coefficients and tool geometry are variable along the tool axis resulting in varying dynamics along the tool axis. In order to take these variations into account, cutting tool is divided into discrete disc elements with height of Δz (Fig. 13). An iterative method is applied for the solution of stability limits where cutting depth (a) is incremented by steps of ΔA. For the cutting depth a, the number of disc elements m that are in cut with the workpiece is determined using the engagement model [Ozturk, 2007]. The iteration continues until the calculated limiting cutting depth (a_{lim}) is less than the cutting depth (a).

The cutting forces in TCS on the j^{th} flute on a disc element l can be expressed for local immersion angle φ_j as follows (Fig. 13):

$$\begin{bmatrix} F_x^l(\varphi_j) \\ F_y^l(\varphi_j) \\ F_z^l(\varphi_j) \end{bmatrix} = \mathbf{T_{xyz}} \begin{bmatrix} K_{rc}(\varphi_j) \\ K_{tc}(\varphi_j) \\ K_{ac}(\varphi_j) \end{bmatrix} h_d \Delta \frac{\Delta z}{\sin K} \tag{5}$$

where T_{xyz} is the transformation matrix that transforms radial, tangential and axial forces to x, y and z directions and K is the axial immersion angle.

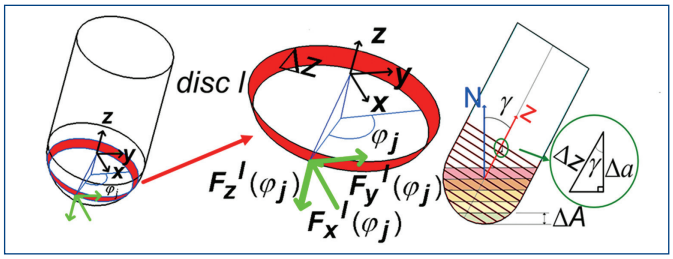

Figure 13. *Dynamic cutting forces on discrete elements*

Height of disc elements Δz needs to be written in terms of the disc height along the surface normal direction Δa (Fig. 13) since cutting depth (a) is defined in the surface normal direction in 5-axis milling:

$$\Delta z = \frac{\Delta a}{\cos\gamma} \tag{6}$$

where γ is the inclination angle which exists between the tool axis (z) and surface normal axis (N) due to lead angle (l_e) and tilt angle (t_i) (Fig. 13). It is calculated using the following equation:

$$\gamma = \cos^{-1}\left[\cos(l_e)\cos(t_i)\right] \tag{7}$$

Defining a new $B^{lj}(\varphi_j)$ matrix as follows:

$$\mathbf{B}^{lj}(\varphi_j) = \frac{1}{\cos\gamma \sin K}\mathbf{T}_{\mathbf{xyz}}\begin{bmatrix} K_{rc}(\varphi_j) \\ K_{tc}(\varphi_j) \\ K_{ac}(\varphi_j) \end{bmatrix}\mathbf{u} \tag{8}$$

Summing the cutting forces contributed by all the teeth on disc element *l*, total dynamic forces at reference immersion angle φ are found from equation (5) as follows:

$$\begin{bmatrix} F_x^{\,l}(\varphi) \\ F_y^{\,l}(\varphi) \\ F_z^{\,l}(\varphi) \end{bmatrix} = \Delta a \mathbf{B}^l(\varphi)\begin{bmatrix} \Delta x_d \\ \Delta y_d \\ \Delta z_d \end{bmatrix} \tag{9}$$

where $B^l(\varphi)$ is the summation of $B^{lj}(\varphi_j)$ for all *n* teeth.

Directional coefficient matrix $B^l(\varphi)$ can be represented by Fourier series expansion. However, Ozturk and Budak [2008] showed that only the first term in the expansion, i.e. single frequency solution, is sufficient to obtain accurate predictions. For this case $B_0^{\,l}$ is a time invariant but immersion dependent coefficient matrix, and it can be calculated by averaging the $B^l(\varphi)$ in a tooth period:

$$\mathbf{B}_o^{\,l} = \frac{1}{\varphi_p}\int_o^{\varphi_p}\mathbf{B}^l(\varphi)d\varphi \tag{10}$$

where φ_p is the pitch angle between the flutes.

Then dynamic displacement vector is defined as follows:

$$\begin{bmatrix} \Delta x_d \\ \Delta y_d \\ \Delta z_d \end{bmatrix} = (1-e^{-i\omega_c\tau})\mathbf{G}(i\omega_c)\begin{bmatrix} F_x(t) \\ F_y(t) \\ F_z(t) \end{bmatrix} \tag{11}$$

$F_x(t)$, $F_y(t)$, $F_z(t)$ are dynamic cutting forces in TCS coordinate system. **G** is the transfer function matrix oriented with respect to the TCS coordinate system [Ozturk 2007]. In cases where both cutting tool and workpiece are flexible, the transfer function matrix **G** is equal to the summation of individual transfer function matrices of the cutting tool and the workpiece.

After performing necessary substitutions into the equation (11), the dynamic cutting forces provide the following eigenvalue problem:

$$\begin{bmatrix} F_x \\ F_y \\ F_z \end{bmatrix} e^{i\omega_c t} = \Delta a(1-e^{-i\omega_c\tau})\left(\sum_{l=1}^{m}\mathbf{B}_\mathbf{0}^{\,l}\right)\mathbf{G}(i\omega_c)\begin{bmatrix} F_x \\ F_y \\ F_z \end{bmatrix} e^{i\omega_c t} \tag{12}$$

where *m* is the total number of disc elements in the analysis. Equation (12) has non-trivial solutions if and only if the following determinant is equal to zero:

$$\det\{\mathbf{I} + \lambda\mathbf{\Phi}\} = 0 \tag{13}$$

where Φ and complex eigenvalue λ are defined as follows:

$$\lambda = -\Delta a(1-e^{-i\omega_c\tau}) = \lambda_R + i\lambda_I$$
$$\mathbf{\Phi} = \left(\sum_{l=1}^{m}\mathbf{B}_\mathbf{0}^{\,l}\right)[G(i\omega_c)] \tag{14}$$

Substituting $e^{-i\omega_c\tau} = \cos\omega_c\tau - i\sin\omega_c\tau$ into equation (14) (14), the following relation is obtained [Ozturk 2010]:

$$\lambda_I(1-\cos\omega_c\tau) = \lambda_R\sin\omega_c\tau \tag{15}$$

Defining

$$\kappa = \frac{\lambda_I}{\lambda_R} = \frac{\sin\omega_c\tau}{1-\cos\omega_c\tau}$$

the elemental critical depth Δa_{lim} can be found as:

$$\Delta a_{\text{lim}} = -\frac{1}{2}\lambda_R(1+\kappa^2) \tag{16}$$

Since there are *m* discs in the analysis, limiting cutting depth (a_{lim}) at chatter frequency ω_c is determined as follows:

$$a_{\text{lim}} = -\frac{m}{2}\lambda_R(1+\kappa^2) \tag{17}$$

Once the limiting cutting depths are calculated for each chatter frequency in the chatter frequency range, the corresponding spindle speeds can be calculated as proposed in [Budak 1998].

4.2 Verification tests

The workpiece material is a rectangular block of AISI 1050 steel. Helix angle and radial rake angle on the 2 flute ball-end mills are 30° and 8°, respectively. The feed rate is 0.05 mm/tooth in the both examples.

Cutting force coefficients are calculated using the *mechanics of milling* method [Budak 1998]. An orthogonal database consisting of chip thickness ratio (r_t), friction angle (β) and shear stress (t_{shear}) is generated for AISI 1050 steel based on the uncut chip thickness *ct* (mm) and the cutting speed *V* (m/min):

$$r_t = 0.4 + 0.0005V + 0.6ct$$
$$\beta = 26.8 - 0.0313V + 11.77ct\ (\text{deg}) \tag{18}$$
$$\tau_{shear} = 450.3 + 0.4V + 227.5ct\ (\text{MPa})$$

In the first example, the cutting tool is an 8mm diameter ball-end mill which is connected to the tool holder with a shrink fit holder and overhang length of it is 54.6 mm. The process is a following cut operation where cross-feed direction is positive and step over is 0.1mm. Lead and tilt angles are both 15°. The measured FRFs are modified to compensate for the accelerometer's mass, which is 0.7 grams, using the formulation in [Ozsahin 2010]. The measured FRFs in X and Y directions are nearly the same. Hence, Tab. 2 represents the modal data for both X and Y directions.

	Mass modified modal data		
Mode #	**f_n(Hz)**	**ζ(%)**	**m(kg)**
1	1826.7	0.99	0.0418
2	1934.4	0.96	0.0824
3	2028.4	0.97	0.0852

Tab. 2. *Modal data for 8 mm ball-end mill*

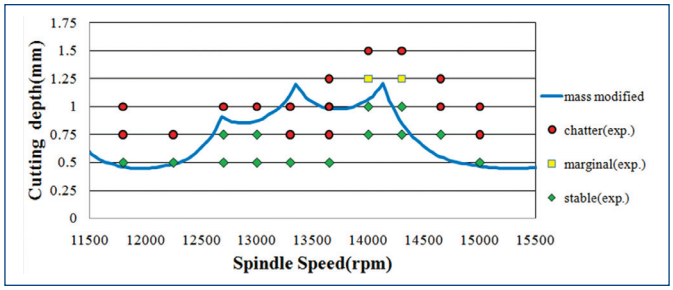

Figure 14. *Stability diagram for the example case*

The stability diagram predicted using the mass modified modal data with single-frequency solution is shown in Fig. 14 together with the experimental results. It is seen that the agreement between the

single-frequency solution method and the experimental results are reasonable.

Simulated effects of lead and tilt angles on absolute stability limit are presented in Fig. 15. Rotary axes affect the stability limits due to two reasons. First, they affect the tool-workpiece engagement zone, dynamic cutting forces, and thus stability limits. Lead and tilt angles may also affect the feed direction depending on the machine tool configuration. In such a case the FRFs must be oriented in the feed direction which also affects the eigenvalues of the characteristic equation, and therefore the stability limit. Fig. 15 shows that these angles have considerable effect on stability for the case considered.

Using the presented stability models, effect of lead and tilt angles on absolute stability limits are demonstrated on another example case. It is a slotting operation and the cutting tool is a 20 mm diameter ball-end mill. The tool is connected to the tool holder with a power chuck system where the overhang length is 62.3 mm. The measured modal data of the cutting tool is presented in Tab. 3. The other process parameters are the same as the ones in the first example. The mass of the accelerometer has negligible effect on the measured FRF in this case.

Direction	f_n(Hz)	ζ (%)	k (N/mm)
X	747.3	3.89	26300
Y	766	3.98	36000

Tab. 3. *Modal data for the second case*

In order to compare these results with experiments, three different lead and tilt combinations; (15°, 15°), (0°, 0°), (0°, 30°) are selected. For these three cases, the absolute stability limits are determined experimentally and shown on Fig. 15, as well. Comparing the simulation and experimental results, it can be concluded that the proposed models predict the effect of lead and tilt angles on stability limits with a reasonable accuracy. Therefore, the stability model can also be used to determine the lead and tilt angles which result in higher chatter limits.

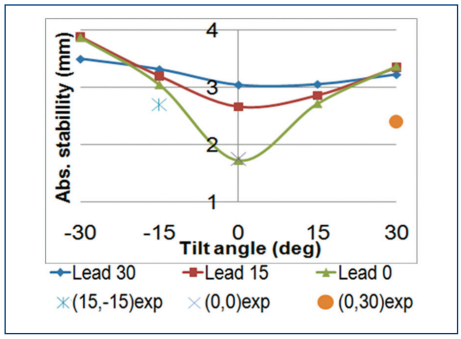

Figure 15. *Effect of lead and tilt angle on absolute stability*

5. 5-axis milling cycle simulation

In order to be able to simulate 5-axis machining cycles, dexel based Z-mapping method is used to determine the engagement boundaries along a milling cycle and to update the in-process workpiece (IPW), where the details are summarized in Fig. 16. The rough workpiece information is obtained in STL format, whereas the cutting tool information is obtained using the standard tool definition. Then, the workpiece geometry is converted into bunch of vectors on an equally spaced grid, storing the Z values of the workpiece geometry. In order to handle the 5-axis motion the vectors are divided in Z-direction, as well. The solid model of the cutting tool is generated by revolving the cross section contour around its axis.

The position and orientation of the cutting tool is parsed from the CL file, where *x, y,* and *z* coordinates of the tool tip and *i, j, k* components of the unit tool axis vector are provided as shown in. It is required to translate and orient the points according to the tool position and tool axis at each tool move.

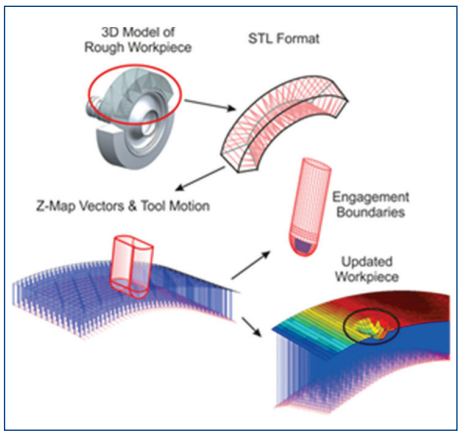

Figure 16. *Application of Z-map method and modeling of tool motion*

6. Application

The application of the modeling and the simulation methods are demonstrated on 5-axis flank mill roughing of a gas turbine engine compressor made out of Ti6Al4V. The simulated cycle cutting geometry is shown in Fig. 17.a. First, the roughing operation is optimized using force simulations. Then, the chatter stability analyses are used to select tooling and milling conditions for finishing.

6.1 Optimization of roughing cycle

Feed rate scheduling is applied to keep the maximum bending force acting on the tool at a predefined level as shown in Fig. 17b. It is observed that the maximum bending force in one revolution of the tool, Fxy, varies from 3000 N to 6500 N. These are very high forces which may cause tool breakage. Thus, the feed rate scheduling is applied to level the force at 6000 N, where the scheduled and

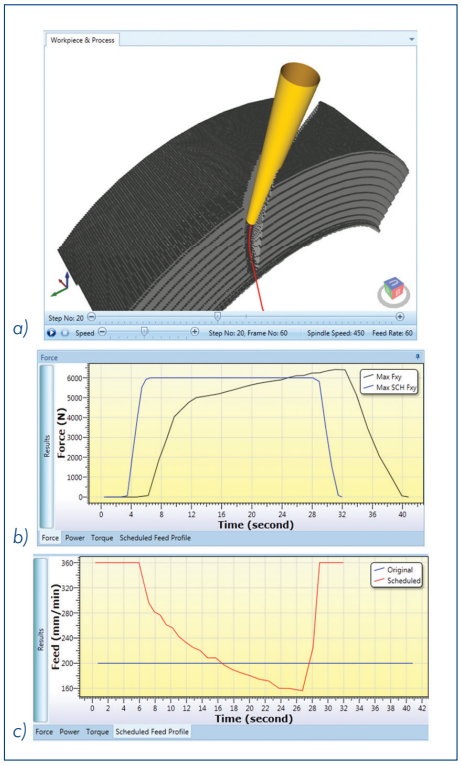

Figure 17. *Example 5-axis milling application (a) Simulated cycle (b) Simulated maximum bending force for constant and varying feed rates (c) Original and scheduled feed rate profiles*

original feed profiles are plotted in Fig. 17c. It is clearly seen that almost 20% of time saving is obtained through feed scheduling.

6.2 Chatter stability of finishing

The measured FRF's for three cutting tools which can potentially be used fare given in Fig. 18. The corresponding simulated stability diagrams are given in Fig. 19a. It is seen that Tool 26 provides higher stability limit for the finishing pass. The machined surfaces are shown in Fig. 19c. where a good agreement is observed with the stability diagrams. There are slight chatter marks due to workpiece vibrations at the upper portions of the surface finished with Tool 26 due to the workpiece vibration modes. The dynamics of the workpiece is more challenging to be included in the analysis due to structural properties during machining. However, Budak [2012] demonstrated that workpiece dynamics and its continuous variation can be modeled accurately using structural modification methods. They demonstrated the application of the method on a compressor blade similar to the one used here.

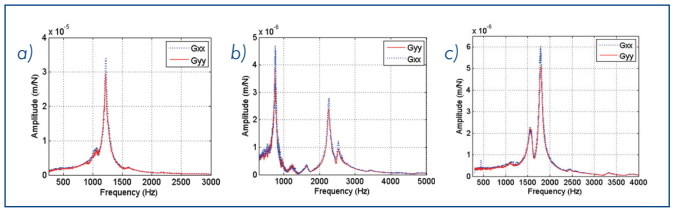

Figure 18. *Measured FRF's for Tool (a) 22, (b) Tool 25 and (c) Tool 26*

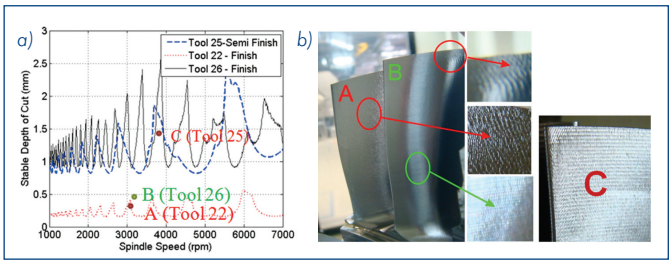

Figure 19. *(a) Stability diagrams, (b) Surface finish by Tool 22 (A-severe chatter), Tool 25 (C-chatter), Tool 26 (B-stable)*

7. Conclusions

An overview of 5-axis milling geometry and process mechanics is given in this paper. Milling force and stability models are presented for 5-axis milling using ball-end milling tools. It is shown that the process conditions can be optimally selected by the help of these models for increased productivity. Implementation of the models in a simulation platform using graphical interfacing with the tool path is also demonstrated for optimization of complete continuous 5-axis milling cycles.

References

[Altintas 1999] Altintas, Y. et al. Analytical Prediction of Stability Lobes in Ball End Milling, Trans. ASME Journal of Manufacturing Science and Engineering, 1999, Vol. 121, pp. 586–592.

[Budak 1996] Budak, E. et al. 1996, Prediction of Milling Force Coefficients from Orthogonal Cutting Data, Trans. ASME Journal of Manufacturing Science and Engineering, 1996, Vol.118, pp. 216–22.

[Budak 1998] Budak, E. and Altintas, Y. Analytical Prediction of Chatter Stability in Milling. Part I: General Formulation, Trans. ASME Journal of Dynamic Systems, Measurement and Control, 1998, Vol. 120, pp. 22–30.

[Budak 2009] Budak, E. et al., Modeling and Simulation of 5-Axis Milling Processes, CIRP Annals-Manufacturing Technology, 2009, Vol. 58, No.1, pp. 347-350.

[Budak 2012] Budak, E. et al., Prediction of Workpiece Dynamics and its Effects on Chatter Stability in Milling, CIRP Annals-Manufacturing Technology, 2012, Vol. 61/1, pp. 2012.

[Engin 2001] Engin, S. and Altıntaş, Y. Mechanics and Dynamics of General Milling Cutters. Part I: Helical End Mills, Int. Journal of Machine Tools and Manufacture, 2001, Vol. 41, No. 15, pp 2195–2212.

[Fussel 2003] Fussell, B.K. et al. Modeling of Cutting Geometry and Forces for 5 axis Sculptured Surface Machining, Computer Aided Design, 2003, Vol. 35, pp. 333-346.

[Gong 2009] Gong, H. and Wang, N. Analytical Calculation of the Envelope Surface for Generic Milling Tools Directly from CL-data Based on the Moving Frame Method, Computer Aided Design, 2009, Vol. 41, pp. 848–855.

[Kaymakci 2006] Kaymakci L. et al. 2006, Machining of Complex Sculptured Surfaces with Feed Rate Scheduling, International Journal of Manufacturing Research, 2006, Vol. 1, No. 2, pp. 157–175.

[Kim 2000] Kim, G.M. et al. Cutting Force Prediction of Sculptured Surface Ball-end Milling Using Z-map, International Journal of Machine Tools & Manufacture, 2000, Vol. 40, pp. 277–291.

[Larue 2005] Larue, A. and Altintas, Y. 2005, Simulation of Flank Milling Processes, International Journal of Machine Tools and Manufacture, 2005, Vol. 45, pp. 549-559.

[Lazoglu 2003] Lazoglu, I. Sculptured Surface Machining: A Generalized Model of Ball-end Milling Force System, International Journal of Machine Tool and Manufacture, 2003, Vol. 43, pp. 453–462.

[Lazoglu 2009] Lazoglu, I. et al. 2009, Tool Path Optimization for Free Form Surface Machining, CIRP Annals-Manufacturing Technology, 2009, Vol. 58, No. 1, pp. 101–104.

[Lopez De Calla, 2007] Lopez De Lacalle et al. Toolpath Selection Based on the Minimum Deflection Cutting Forces in the Programming of Complex Surfaces Milling, 2007, International Journal of Machine Tool and Manufacture, Vol.47, pp. 388–400.

[Ozkirimli, 2011] Ozkirimli, O. M. and Budak, E. Process Simulation for 5-Axis Machining for Generalized Milling Tools, International Journal of Design Engineering, special issue: Advanced Methods for Virtual Machine Design and Production, 2011, Vol. 3, No. 3, pp. 232–246.

[Ozsahin 2010] O. Özşahin et al. Analysis and Compensation of Mass Loading Effect of Accelerometers on Tool Point FRF Measurements for Chatter Stability Predictions, Int. J. Machine Tools and Manufacture, 2010, Vol. 50, No. 6, pp. 585–589.

[Ozturk, 2006] Ozturk, B. and Lazoglu, I. Machining of Free Form Surface. Part I: Analytical Chip Load, International Journal of Machine Tools and Manufacture, 2006, Vol. 46, pp. 728–735.

[Ozturk, 2007] Ozturk, E. and Budak, E. Modeling of 5-Axis Milling Process, Journal of Machining Science and Technology, 2007, Vol. 11, No. 3, pp. 287–311.

[Ozturk, 2009] Ozturk, E. et al. Investigation of Lead and Tilt Angle Effects in 5-Axis Ball-End Milling Processes, International Journal of Machine Tools and Manufacture, 2009, Vol. 49, No. 14, pp. 1053–1062.

[Ozturk, 2010] Ozturk, E. and Budak, E. Dynamics and Stability of 5-Axis Ball-end Milling, Trans. ASME Journal of Manufacturing Science and Technology, 2010, Vol. 132, 021003 (12 pages).

[Roth, 2007] Roth, D. et al. Mechanistic Modelling of 5-axis Milling Using an Adaptive and Local Depth Buffer, Computer-Aided Design, 2007, Vol. 37, pp. 302–312

[Shamoto, 2009] Shamoto, E. and Akazawa, K. Analytical Prediction of Chatter Stability in Ball End Milling with Tool Inclination, CIRP Annals-Manufacturing Technology, 2009, Vol. 58, pp. 351–354.

[Zhu, 2001] Zhu, R. et al. Mechanistic Modelling of the Ball-end Milling Process for Multi-axis Machining of Free-form Surfaces, Journal of Manufacturing Science and Engineering, 2001, Vol. 123, pp. 369–379.

Contacts

Manufacturing Research Lab, Sabanci University
Tuzla İstanbul 34956, Istanbul, Turkey
e-mail: ebudak@sabanciuniv.edu